INNOVATION FOREVER
Open Access

Innovation Discovery
ISSN 2959-5150 (Online)

Research Article

Anti-corrosion Properties of Functionalized Organo-silane Coupling Agents for Galvanized Steel

Sukanta Badaik[1,2], Mausumi Ray[1], Rishav Ghosh[3], Monika Nidhi[4], Suryakanta Nayak[1], Amar Nath Bhagat[1], Balram Ambade[2], Suryanarayana Reddy Minnam Reddy[5], Tapan Kumar Rout[1*]

[1]*R&D, Surface Engineering Research Group, Tata Steel Limited, Jamshedpur, India*
[2]*Department of Chemistry, National Institute of Technology Jamshedpur, Jamshedpur, India*
[3]*Department of Materials Science, Monash University, Melbourne, Australia*
[4]*Tata Quality Management, Tata Steel Limited, Jamshedpur, India*
[5]*Product Application Group, Tata Steel Limited, Bangalore, India*

[*]***Correspondence to: Tapan Kumar Rout, PhD, Professor,*** *R&D, Surface Engineering Research Group, Tata Steel Limited, Jamshedpur, 831001, India; E-mail: tapankumarrout@tatasteel.com*

Abstract

Silane precursor selection is an important criterion for achieving great anticorrosive performance on steel substrates using sol-gel technology. A density functional theory (DFT) study was performed on functional and nonfunctional organosilane precursors. The global reactivity parameters, such as the global hardness (η), dipole moment (μ), and number of electrons transferred (ΔN) to the metal substrate, were calculated to identify suitable silane coupling agents. DFT studies revealed that precursors containing functional groups such as epoxy, amine, and mercapto offer better protection against corrosion to galvanized steel by providing stronger interfacial adhesion than precursors without functional moieties. The DFT-calculated adsorption energy (E_{ads}) is more than 40.0kcal/mol for the adsorption of functional organosilanes onto the $(ZnO)_{12}$ cluster. Evidence of chemical bond formation at the interface for functional organosilanes is found in the electron density overlap in the MOs. Natural charge analyses revealed clear charge transfer from the organosilane moiety to the $(ZnO)_{12}$ cluster. The theoretical predictions were validated via experiments. Electrochemical studies demonstrated a protective efficiency of 92.5% for Ie with an impedance of 92.9kΩ·cm^2. The presence of the respective functional groups and surface morphology were evaluated by FTIR and SEM. The order of corrosion inhibition of organosilanes was found to be MPTMS≈APTES>GPTMS>TEOS.

Keywords: sol-gel coating, organosilane, galvanized steel, anti-corrosion; density functional theory

Received: August 7, 2024
Revised: October 10, 2024
Accepted: November 7, 2024
Published: November 11, 2024

Citation: Badaik S, Ray M, Ghosh R, Nidhi M, Nayak S, Bhagat AN, Ambade B, Reddy SRM, Rout TK. Anti-corrosion Properties of Functionalized Organo-silane Coupling Agents for Galvanized Steel. *Innov Discov*, 2024; 1(4): 32.

1 INTRODUCTION

Galvanized (GI) steel is a conventional steel coated with zinc via a process called galvanization. This zinc coating acts as a corrosion-resistant barrier, increasing the durability and performance of the underlying steel substrate. GI steel is utilized in the automobile sector because of its superior strength-to-weight ratio, formability, and dent resistance. The presence of a thin oxide film on the surface might serve as an initiating point for coating failure due to insufficient interfacial adhesion. This weak area initiates corrosion, which can be slowed by applying a coating to the surface. The surface coating can act (i) as a physical barrier, (ii) as a cathodic protector of the substrate by acting as the sacrificial anode or (iii) as a passivating layer (anodic protection)[1,2]. Chrome-based chemical passivation coatings have been predominantly applied to steel to obtain superior corrosion resistance and good adhesion with the substrate[3]. However, due to environmental regulations imposed as a result of the carcinogenic effect of hexavalent chromium in such coatings, research has focused on developing alternative coating technologies[4]. The sol-gel process is one such evolving coating technology capable of providing corrosion resistance,

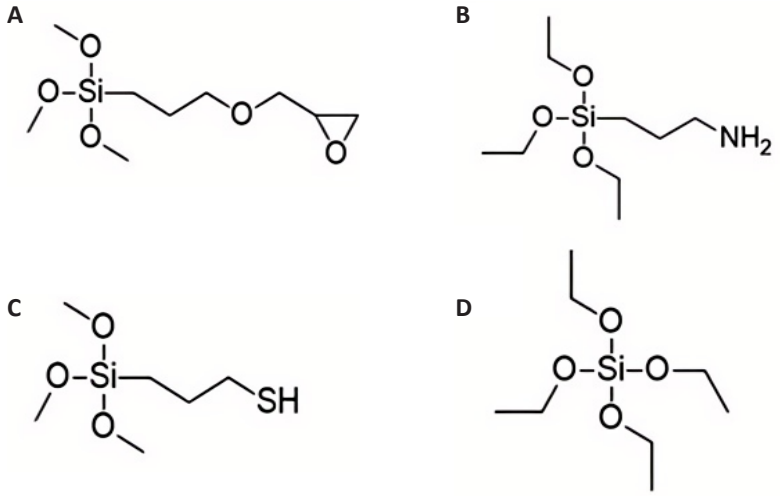

Figure 1. Molecular Structures of (A) GPTMS, (B) APTES, (C) MPTMS, and (D) TEOS.

mechanical and wear durability with low volatile organic compounds (VOCs) and negating the usage of chromates[5]. Water- and/or alcohol-soluble alkoxide precursor materials and dopant ions may be easily included in such sols due to their simple synthesis and wet-chemical method of coating deposition, resulting in enhanced coating characteristics.

Due to the use of sol-gel technology, organosilanes have gained popularity in thin-organic coating research and have been used as chromate substitutes. These silane-based compounds are typically organofunctional alkoxysilanes, $(RO)_3$-Si-R′, where OR is a hydrolyzable alkoxy group and R′ is a nonhydrolyzable organofunctional group, which may include an amine group ($-NH_2$), epoxy group (-C-O-C), thiol group (-SH), etc[6]. The organic moiety (-R) enhances the flexibility, toughness, and cross-linking density of the coating network while also allowing functional compatibility with an organic polymer in a coating/paint system. On the other hand, the inorganic moiety (R-O-Si) aids in the attachment of silane molecules to the metal substrate. The alkoxy groups (RO-) at one end of the molecule are hydrolyzed to silanol groups (H-O-Si), which engage with the hydroxide groups on the metal substrate to generate a Si-O-M covalently bonded metal/film interface[7]. However, after curing the silane layer, it crosslinks to a Si-O-Si siloxane network-like structure, acting as a barrier to prevent corrosive ions from accessing the steel. While most studies have been conducted to determine how silane coatings resist corrosion, only a few studies, such as van Ooij's, have focused on understanding the influence of functional and nonfunctional groups on the corrosion performance of such silanes[8]. Functional silanes often work as additional coupling agents for paint layers since the functional group creates chemical bonds with the polymer resin[9,10].

The adhesion of silanes to basic substrates has been partially clarified by experiments, but a deep understanding of interactions between coating molecules and metals is crucial for developing effective anticorrosion coatings. Predicting chemical reactivity remains one of chemistry's most difficult challenges. By determining the electronic structures, quantum chemistry calculations have been shown to be a very useful technique for assessing the reactivity of molecules and their potential to shield the metal from corrosion[11-16]. With this method, the corrosion resistance performance of the coating molecule can be projected by calculating global reactivity parameters. The calculation of the binding energy between the coating ingredient and substrate explicitly sheds light on the interfacial bonding mechanism and provides quantitative information about the interfacial adhesion of the coating ingredient to the substrate. The literature in these regards focuses primarily on the molecular structure and adhesion of coating ingredients for the corrosion protection of metal substrates[17]. There is a lack of relevant literature on the fundamental understanding of the corrosion performance of organosilanes toward GI steel using quantum chemistry methods, especially studies on the explicit interactions between organosilanes and substrates. The present work focuses on clarifying the corrosion protection properties and interfacial adhesion mechanism of functional and nonfunctional organosilanes using quantum chemical studies and experimental studies. Here, density functional theory (DFT) was used for quantum chemical studies.

The current study engrossed on understanding the surface protection efficiency of different functional organosilanes, viz. 3-Glycidoxypropyltrimethoxysilane (GPTMS), 3-merc aptopropyltrimethoxysilane (MPTMS), and nonfunctional organosilanes, viz. tetraethoxysilane (TEOS), as shown in Figure 1, respectively, on GI steel. In the DFT study, model compounds of GPTMS, 3-aminopropyltriethoxysilane (APTES), MPTMS, and TEOS were employed, where the OCH_3 group in GPTMS (Figure 1A) and MPTMS (Figure 1C) and the OCH_2CH_3 group in APTES (Figure 1B) and TEOS (Figure 1D) attached to the center Si atom are replaced with OH groups to reduce the computational time because the OMe/OEt groups connected to the Si atoms lastly convert

Table 1. Sample ID and composition of coating solutions

Sample ID	Coating Solution
1T	5 vol % TEOS in water-ethanol ratio=1:4 (v/v)
1G	5 vol % GPTMS in water-ethanol ratio=1:4 (v/v)
1A	5 vol % APTES in water-ethanol ratio=1:4 (v/v)
1M	5 vol % MPTMS in water-ethanol ratio=1:4 (v/v)

to OH groups during the process of hydrolysis. These model complexes of GPTMS, APTES, MPTMS, and TEOS are denoted as 1G, 1A, 1M, and 1T, respectively. The DFT-calculated results were experimentally validated through electrochemical studies. In the hot dip galvanizing process, a thin, insoluble ZnO layer forms on the surface as needle-like nanowires within 48 hours of atmospheric exposure. This ZnO layer, with a thickness of nanometer order, corrodes very slowly, thereby protecting the underlying galvanized coating[18-20]. As a result, the uppermost ZnO layer serves as a shield, shielding the base iron behind the galvanized layer from the elements. This ZnO layer also reacts with coatings and paints that have been applied. This work used DFT to investigate the atomic-level reactivity of 1G, 1A, 1M, and 1T molecules with GI steel. The uppermost ZnO nanolayer of GI steel was modelled using the $(ZnO)_{12}$ nanocluster[21]. DFT was employed to investigate the interfacial adhesion mechanism of organosilane precursors with $(ZnO)_{12}$ nanoclusters.

2 MATERIALS AND METHODS

2.1 Experimental Section

2.1.1 Synthesis of the Silane Coating Solution

APTES, MPTMS, GPTMS, and TEOS of 98% purity were purchased from Sigma–Aldrich. Distilled water and ethanol were employed as coating solution media, while glacial acetic acid was used as a silane hydrolysis reaction initiator.

2.1.2 Substrate Preparation

A GI steel sheet was used as the substrate for the coating application, where the zinc coating thickness was ~10µm. A coupon sample with a thickness of 0.8mm and a surface length and width of 100mm and 30mm, respectively, was used for coating and further experimentation. These substrates were degreased in a 2.5wt.% Ridoline 1352BA (purchased from M/S Henkel Corporation) solution at 65°C for 1-2min, followed by rinsing in distilled water and hot air drying before coating.

2.1.3 Synthesis of the Silane Coating Solution

Four different coating solutions were prepared by varying the silane concentration and water-ethanol ratio (v/v). The abovementioned silane chemicals (5 vol%) were poured into a 1:4 (v/v) ratio of the waterethanol mixture. Glacial acetic acid was mixed with each coating solution dropwise until the pH was in the 5-6 range. The solution was then agitated for an additional 48h to facilitate complete hydrolysis of the silanes. This hydrolyzed silane solution was then used for coating deposition. The composition and sample IDs of each coating solution are presented in Table 1.

2.1.4 Coating Deposition and Curing

After the steel samples were cleaned, they were dipped into the silane solution for 60sec before being dried in a hot air oven for 5min at 120 degrees Celsius to create a hardened coating. This is an industrial process for coating steel surfaces in many plants.

2.1.5 Fourier Transform Infrared (FTIR) Spectroscopy

FTIR studies were performed on both the hydrolyzed silane solution and the final cured coating to determine the structural changes, such as the extent of hydrolysis of the coating solution and the curing of the coating film. A Vertex 80 FTIR System (Bruker, Germany) was used to perform all the FTIR tests. The scan wavenumbers of each test ranged from 450 to 4000cm^{-1}.

2.1.6 Coating Morphology

We investigated the coating surface microstructures of the four coated steel substrates using a ZEISS Crossbeam 350 scanning electron microscope equipped with an energy-dispersive spectrometer at an accelerating voltage of 10kV and a probe current of 2.8A at a working distance of 10mm.

2.1.7 Electrochemical Measurements

We employed a flat three-electrode cell arrangement for the electrochemical testing, with bare and silane-coated GI steel samples serving as the working electrodes, a saturated calomel electrode serving as the reference electrode, and a platinum mesh serving as the counter electrode. A 3.5 wt% aqueous solution of NaCl served as the electrolyte in every investigation. A one-square-centimeter section of the working electrode was exposed for every electrochemical test. To get a steady open circuit potential (OCP), the sample was submerged in the electrolyte solution for 30min prior to potentiodynamic polarization and electrochemical impedance spectroscopy (EIS) experiments. Every test was carried out at a temperature of 25°C in an oxygen-free chamber. Experiments on potentiodynamic polarization were conducted at a scan rate of 0.5mV/s throughout a 500mV range with respect to the OCP. EIS research was done to comprehend the causes of corrosion and the barrier properties of the silane coating on GI steel. Applying a 10mV sinusoidal perturbation at OCP throughout a frequency range of 100kHz to 10MHz allowed for the impedance measurement. Gamry EChem Analyst was utilized to compute electrochemical

parameters by simulating the observed spectra with matching comparable electric circuits[22].

2.2 Computational Details

DFT was utilized to optimize the geometries of all four organosilanes, with the B3PW91 functional[23] being utilized for the exchange-correlation term. Previous theoretical investigations[24–27] have demonstrated that when it comes to accurately replicating the experimental geometry of organosilicon compounds, the B3PW91 functional outperforms the B3LYP[23,24,28,29] functional. The stability of the optimized structures was confirmed by verifying that no imaginary frequencies were present in the equilibrium geometries. Using DFT-optimized geometry, the DFT method was used to assess the orbital energy, total energy, and population fluctuations. In this study, we used the BS-I and BS-II basis sets. In BS-I[30], the LANL2DZ (21/11/41) basis set with effective core potential (ECP) was used for all Zn atoms, and the standard 6-31G(d)[29,31,32] a double zeta basis set was employed for all other atoms. Geometry optimization was performed using the BS-I system. Zn atoms in the BS-II system were based on the Stuttgart-Dresden basis set (311,111/22,111/411) with Effective Core Potential (ECP), whereas all other atoms were based on the triple zeta split valence basis set 6-311G(d). BS-II measurements were made of orbital energy, total energy, adsorption energy, and population changes. BS-II was used to calculate global reactivity parameters such as the energies of the highest occupied molecular orbital (HOMO) and lowest unoccupied molecular orbital (LUMO) of the molecule, the electronegativity (χ), the global hardness (η), the energy gap (ΔE) between the HOMO and LUMO, the dipole moment (μ), and the number of electrons transferred (ΔN) from the coating molecule to the substrate. Furthermore, this study used Tomasi's polarizable continuum model (PCM)[33,34]. We included solvation effects (water) in the theory of self-consistent reaction field (SCRF). Notably, gas-phase geometry optimization was used in the PCM calculations. The Gaussian 16 software program was used to carry out all of these computations. Analysis of the natural bond order (NBO) was performed using a technique provided by Weinhold et al[35]. The chemical potential (μ) and global hardness (η) of a chemical system are given by[36]

$$-\mu = \frac{(I+A)}{2} = \chi \qquad (1)$$

$$\eta = \frac{(I-A)}{2} \qquad (2)$$

The ionization potential is denoted by I, the electron affinity is denoted by A, and χ is the absolute electro-negativity for any system.

The frontier orbital energies are determined by Koopman's theorem[30]:

$$-E_{HOMO} = I \qquad (3)$$

$$-E_{LUMO} = A \qquad (4)$$

Until the chemical potentials are equal, electrons will flow from the atom with the lower value in the bulk metal to the atom with the higher value in the coated molecule. The formula for the amount of electrons transported, denoted by "ΔN"[37,38] is:

$$\Delta N = \frac{\chi_{ZnO} - \chi_{mol}}{2(\eta_{ZnO} + \eta_{mol})} \qquad (5)$$

where the absolute electronegativity of zinc oxide in GI steel is denoted by χ_{ZnO} and χ_{mol}, respectively, and the hardness of the coating molecule and zinc oxide is indicated by η_{ZnO} and η_{mol}. The $(ZnO)_{12}$ cluster's χ (5.2eV in gas and 4.1eV in water phases) and η (2.1eV in gas and water phases) were utilized to assess the ΔN values.

3 RESULTS AND DISCUSSION

3.1 Analysis of the Coating Structure

The coating network assemblies after film formation were studied through FTIR and are shown in Figure 2. The presence of multiple peaks in the range of 1000-1130cm^{-1} in the spectrum of the silane films (Figure 2A-D) indicates that Si-O-Si bonds formed due to the curing of all the silane coatings[39]. The peaks in the range of 900-1000cm^{-1} indicate the formation of Si-O-metal bonds[40], which are covalent interactions between the siloxane network and the metal substrate, as shown in Figure 2A-D.

Two peaks in the range of 2830-2950cm^{-1} for silane systems-1G,1 M, and 1A (Figure 2B-D) for both the sol and the film systems represent the -CH_2 asymmetric and symmetric vibrations characteristic of the alkyl chains that exist in all these silanes except for TEOS[41].

The occurrence of a peak at 1255cm^{-1} in the film of the 1G system (Figure 2A) corresponds to an absorption peak of the Si-CH_2 bond in GPTMS[42] while the shoulder peak at 915cm^{-1} can be indicative of the C-O bond of the oxirane ring, which is characteristic of GPTMS[43]. In the case of the 1M system (Figure 2D), a weak peak at 2569cm^{-1} is observed in the sol but is reportedly missing in the film. This weak peak is representative of the thiol group (-SH) of MPTMS[44,45]. Moreover, for the 1A system (Figure 2C), similar weak peaks are observed in the soil in the range of 1550-1600cm$^{-1,}$ which is absent in the film spectrum. The weak amino (-NH_2) peak (1550-1600cm^{-1}) of APTES. The absence of weak peaks in both films (Figure 2C and 2D) could indicate that the bonding to the metal substrate could occur through these groups along with the silanol linkages. Moreover, the occurrence of the 'S' and 'N' atoms in their respective chains would enhance the chances of intramolecular hydrogen bonding and hence allow for a dense, compact siloxane network. Figure 1a shows that a siloxane network formed over the layer on the TEOS-coated steel since only the Si-O-Si peak at 1074cm^{-1} and the Si-O-M peak at 940cm^{-1} were present.

3.2 Surface Morphology of the Coating

Using CB340-EDS (JEOL), scanning electron microscopy

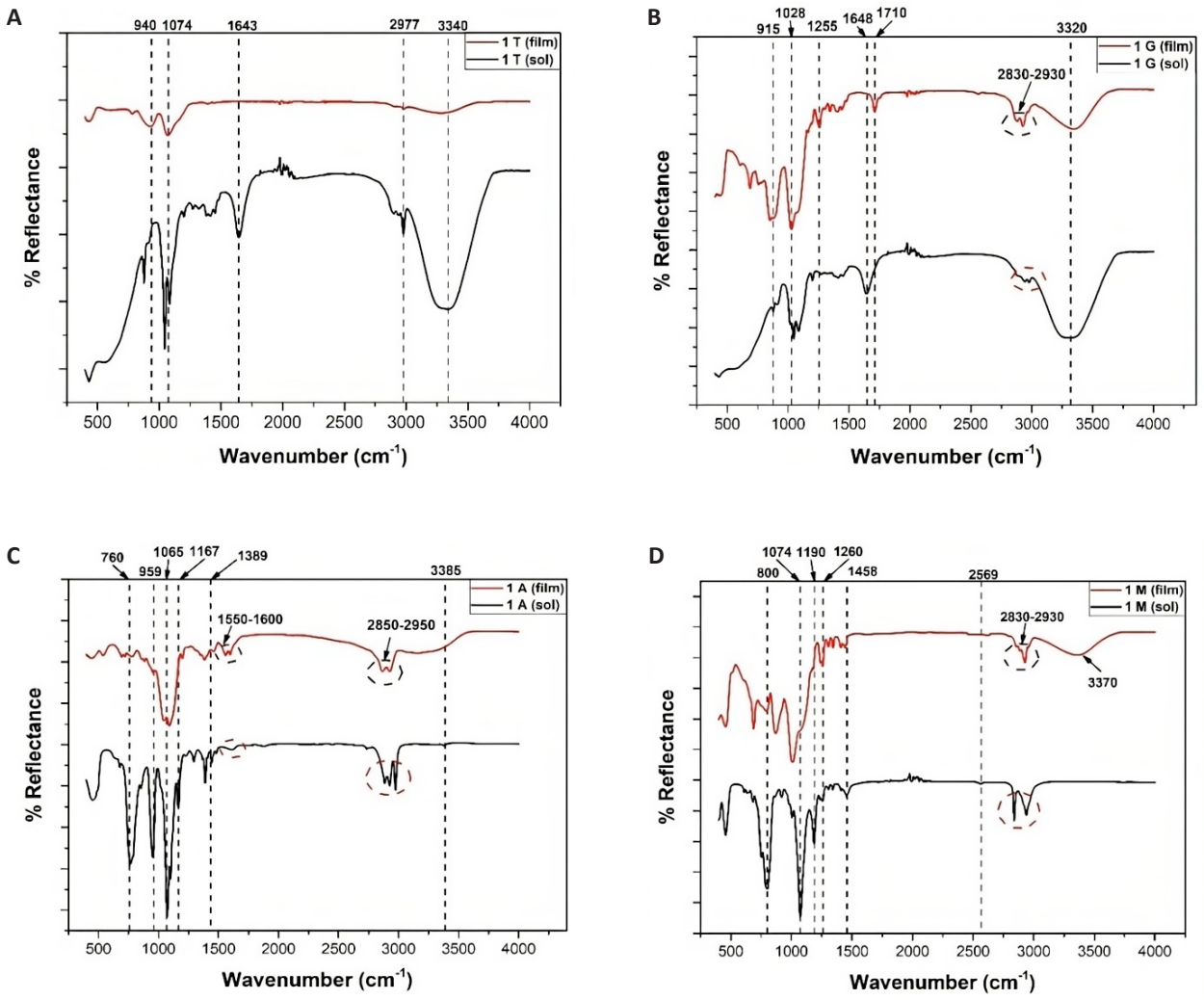

Figure 2. Infrared Spectra for (A) TEOS, (B) GPTMS, (C) APTES, and (D) MPTMS Sol and Coating on GI Steel.

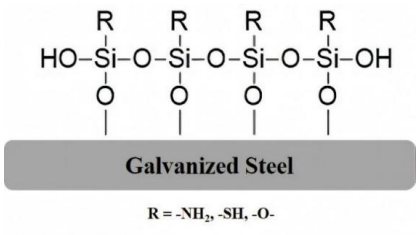

Figure 3. Interaction of the Hydrolyzed Silane Film on Metal Surfaces. R indicates functional groups such as: epoxy, thiol, or amino groups.

(SEM) was used to assess the microstructure of the four organosilane coatings. Figure 3 shows the surface microstructure and cross-sectional appearance of the four different coatings coated on the GI steel substrate. Evidently, a fracture of the coating film was observed for 1T, whereas no such fracture was observed for the other coatings (Figure 4). Following the potentiodynamic polarization study, this is evident for the disintegration of the protection layer for 1T and a path for corroding species to initiate corrosion. In addition, the average coating thicknesses found for 1G, 1A, 1M, and 1T were 13.01, 16.46, 21, and 24.01µm, respectively.

3.3 Electrochemical Results

3.3.1 Potentiodynamic Polarization Studies

We employed a potentiodynamic polarization test in accordance with ASTM G59-97 (2014) to assess the electrochemical behaviour of various coatings in a 3.5% NaCl solution. Using the Tafel extrapolation method, the electrochemical behaviour of the coated substrates was determined by calculating the anodic (β_a) and cathodic (β_c) Tafel slopes, corrosion potential (E_{corr}), and corrosion current density (i_{corr}) from the potentiodynamic polarization curves (Figure 5). Additionally, we evaluated the various parameters using the program Gamry Echem Analyst, as indicated in Table 2. To compare the corrosion resistance characteristics of the various silane-coated films to those of the uncoated steel, the corrosion inhibition efficiency (Ie%)[46], which is specified in equation (6), was determined for each sample.

$$\text{Ie\%} = \frac{i^o_{corr} - i_{corr}}{i^o_{corr}} X\ 100 \qquad (6)$$

where the corrosion current densities of the bare steel and the silane-coated film are denoted by i^o_{corr} and i_{corr}, respectively.

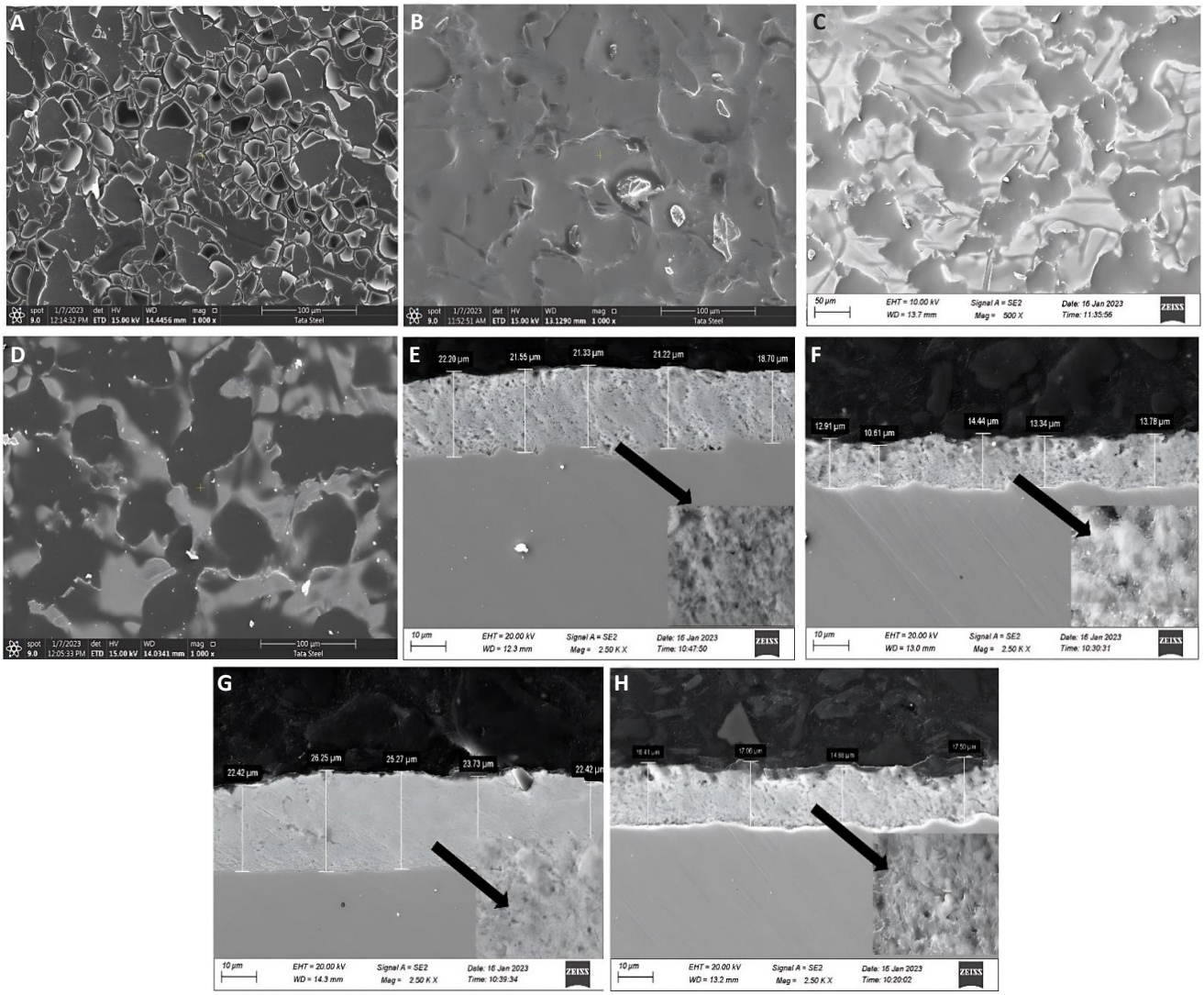

Figure 4. SEM Images of 1T, 1G, 1A, and 1M Coated GI Steel. A-D: Surface microstructure; E-H: Cross-sectional view.

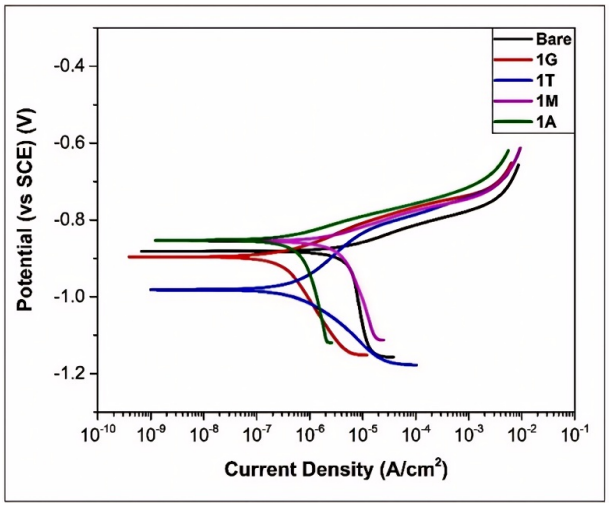

Figure 5. The Potentiodynamic Polarization Graphs for Uncoated and Silane-coated GI Steel.

Figure 5 shows that all the coated steels have similar anodic and cathodic reaction kinetics except for 1T. The 1T coating showed a greater potential shift from that of the bare substrates. All the coated steels show cathodic Tafel slopes higher than the anodic slopes, which can be attributed to the anodic controlled corrosion process. Bare steel shows an even greater cathodic Tafel slope than coated steel. This indicates that the surface is oxidized as soon as it is exposed to electrolyte solutions. Therefore, all the samples show increased anodic dissolution behavior with little increase in the anodic polarization potential. An increased cathodic Tafel slope for coated steel suggests slower cathodic reaction kinetics.

$$2H_2O+O_2+4e \rightarrow 4(OH^-) \qquad (7)$$

It was observed (Table 2) that the corrosion potentials (E_{corr}) of the 1A- and 1M-coated samples shifted toward positive potentials for bare steel, but for 1G and 1T, they shifted toward negative potentials. The combined effect of anodic dissolution and suppression of cathodic reactions can explain the decrease in the corrosion current density[47,48]. The decrease in the corrosion rate as a result of the change in the current density might also be due to the corrosion inhibition offered by the three-dimensional networked silane film[30], which acts as a barrier protective layer against oxygen and chloride ions.

The trend in the corrosion inhibition efficiency values

Table 2. Electrochemical Parameters of Uncoated and Coated Steel Obtained Through Tafel Extrapolation

Samples	E_{corr} (V/SCE)	i_{corr} (μA/cm^2)	β_a (mV/dec)	-β_c (mV/dec)	Ie (%)
Bare GI	-0.892	6.01	57.3	1015	
1T	-0.980	2.19	53.04	632	63.56
1G	-0.886	0.313	70	264	94.79
1A	-0.922	0.339	75	141	94.36
1M	-0.905	0.25	62.4	222	95.84

for the different organosilane formulations proves that functional organosilanes such as 1G (GPTMS), 1M (MPTMS), and 1A (APTES) provide better corrosion protection to GI steel than do nonfunctional organosilanes such as 1T (TEOS). This phenomenon can be explained by the presence of electron-donating groups such as -SH, -NH, and epoxy in the silane system, which allows for better adhesion through coordination bonding to the vacant d-orbital of the metallic zinc coating on the steel[49,50]. Moreover, these organosilanes allow dense film formation by the networked siloxane structure, which can be seen in the microstructure images, but in the case of 1T, the coating film was found to be cracked (Figure 4D). Furthermore, in the case of functional silane coatings, this crosslinked dense film is developed in the process of intramolecular hydrogen bonding within the molecules due to the presence of heteroatoms with different electronegativity. Stronger hydrogen bonding is evident in epoxy-functionalized silane due to the presence of oxygen (O) linkages in the epoxy-functionalized silane (1G) than in amino-functionalized silane (1A). The thiol-functional silane (1M) coating exhibited the best corrosion resistance because of the combined effect of a strong hydrogen-bonded silane network coupled with its inherent corrosion inhibition property, which is further explained by quantum chemical studies in subsequent sections. The mechanisms of interaction were elucidated through DFT calculations and are explained in subsequent sections.

3.3.2 Electrochemical Impedance Spectroscopy Studies

EIS was performed to study the barrier properties and electrochemical reaction phenomena at the coating film and metal interface in 3.5% NaCl aq. Solution[51,52]. The findings from this study supported the observations drawn from potentiodynamic polarization and quantum chemical studies[11,46,53,54]. The Nyquist plots shown in Figure 6A specify the occurrence of dual capacitive loops, which can be further confirmed through two-time constants (in the frequency range of 10^{-1}Hz and 10^{2}-10^{3}Hz), as observed in the corresponding Bode phase angle plot (Figure 6C). The high-frequency spectra are indicative of the barrier qualities of the silane coating, while the low-frequency spectra represent the process of corrosion occurring at the coating-metal contact. Bare steel and silane coatings both exhibit a zone of resistive behavior at higher frequencies (10^{3} to 10^{5}Hz) and a zone of capacitive behavior at low frequencies (10^{-2} to 10^{-1}Hz) in their respective Bode impedance spectra. Compared with that of the coated samples, the resistive behavior at lower frequencies can be most prominently observed in the bare steel. We observed from the Nyquist plot that there was a remarkable increase in the radius of the capacitive loops for the silane coatings on the GI steel sample relative to that on the bare steel sample, indicating a higher protective efficiency of the coated film. The different silane coating films agreed well with the trend observed in the polarization studies. The modulus of the impedance (|Z|) for the different samples (Figure 6B) also corroborates the trend found in the polarization curves. With the intention of better explaining the processes of the electrochemical reactions of the various coating films, we could quantitatively analyze the values of the electrochemical parameters from the impedance spectra. The electrochemical values were calculated by modeling the events occurring at the various interfaces (electrolyte/coating and coating/steel) in an analogous electric circuit and fitting the resulting spectra, as shown in Figure 6D.

The following parts make up the corresponding circuit: (i) electrolytic solution resistance (RS), (ii) silane covering layer resistance (Rc) in parallel with constant-phase element (CPEc), and (iii) at low frequency, constant-phase element (CPEdl) and charge transfer resistance (Rct) corresponding to the corrosion reaction[55–57]. R_c represents the resistance offered by the coating to the penetration of electrolyte and corrosive ions, whereas CPE_c represents the dielectric impedance observed by the coating layer. Constant phase elements were picked to show how different the coatings are physically, and their impedance value is defined as[58]:

$$Z_{CPE} = \frac{1}{(j\omega)^n C} \qquad (8)$$

where j=√-1, C is the capacitance, ω is the angular frequency and is calculated as ω = 2πf·rad·s^{-1}, n is the exponent, which lies in the range between 0 ≤ n ≤ 1. The following formulae were used to convert these constant phase components into capacitive analogs [59]:

$$C = \frac{(CPE \times R)^{1/\beta}}{R} \qquad (9)$$

where R denotes the resistance in parallel or series with the CPE and indicates the constant phase element index (m or n), CPE stands for the constant phase element, and C represents the capacitance. The capacitance values C_c and C_{dl} for the accompanying constant phase

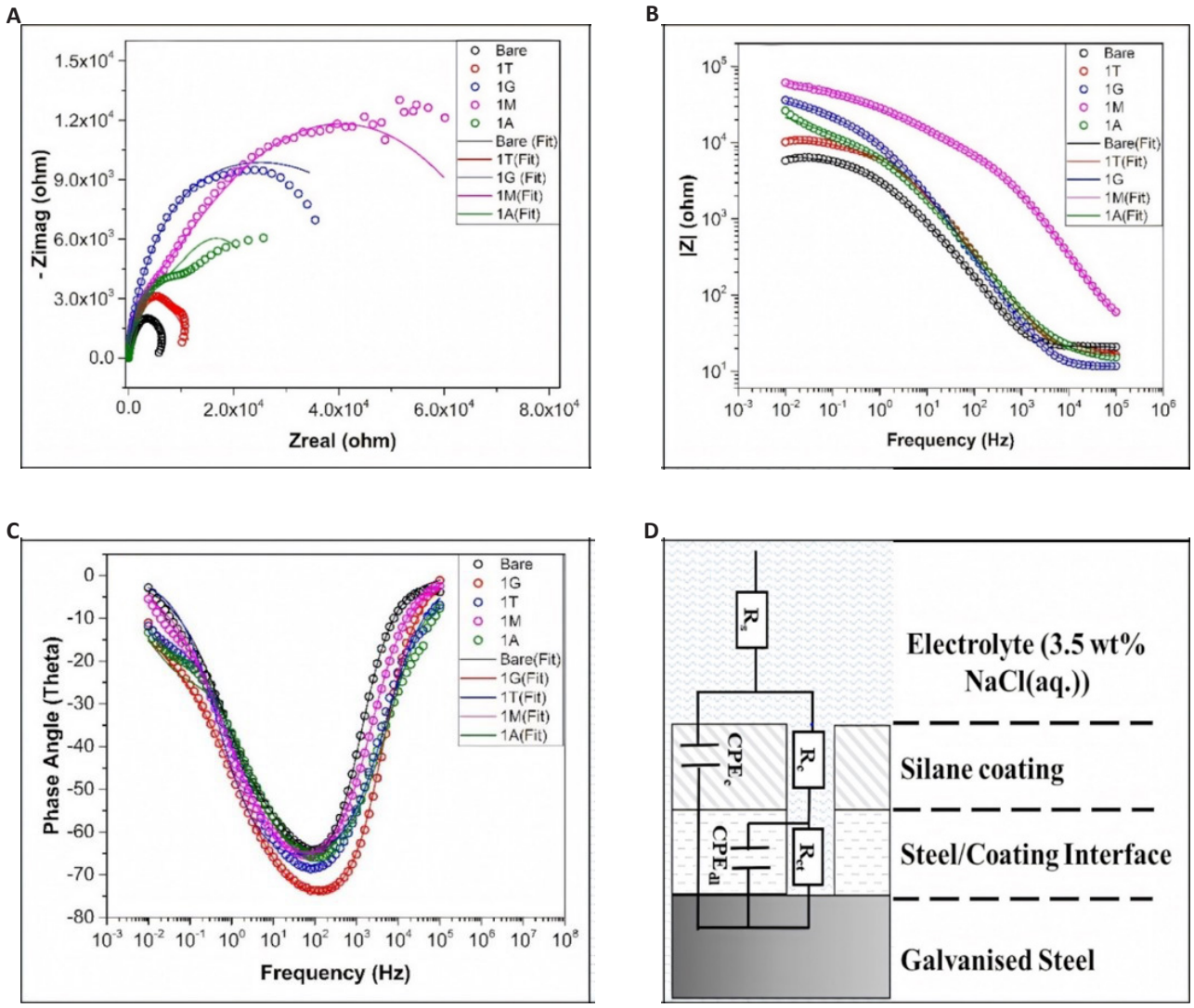

Figure 6. Analyze and Fit the Electrochemical Data of Uncoated and Silane-coated Galvanized (GI) Steel. A: Nyquist, B: Bode-impedance, C: Bode-phase angle plots, D: Electrochemical equivalent circuit with two capacitive elements used to fit the data of uncoated and silane-coated GI steel.

Table 3. The Electrochemical Parameters for Bare and Silane-Coated Gi Steels Obtained Through Eis

Samples	R_s (Ω·cm^2)	R_c (kΩ·cm^2)	C_c (μF·cm^2)	m	R_{ct} (kΩ·cm^2)	C_{dl} (μF·cm^2)	n	R_t (kΩ·cm^2)	CRe (%)
Bare	20.8	0.69	10.4	0.88	0.625	3.41	0.57	6.94	-
1T	19.4	7.00	9.83	0.79	5.34	2.23	0.54	12.3	243.8
1G	19.7	7.58	0.26	0.34	64.2	0.29	0.89	71.7	90.3
1A	18.1	7.03	1.11	0.76	19.4	0.71	0.61	26.4	73.7
1M	20.0	16.01	0.153	0.89	76.9	0.152	0.37	92.9	92.5

elements are displayed in Table 3. The overall resistance provided by the silane coating was computed using the fitted parameters as the sum of the charge transfer (R_{ct}) and coating resistance (R_c).

The corrosion resistance efficiency (CRe) was defined as the impedance to compare the corrosion resistance of the different silane-coated samples to that of the bare steel.

$$\mathrm{CRe}\% = \frac{R_t^o - R_t}{R_t^o} X\ 100 \qquad (10)$$

where R_t^o and R_t represent the resistance to corrosion offered by bare steel and silane-coated steel, respectively. The collected impedance parameters are shown in Table 3.

The value of R_t indicates the resistance to corrosive ions penetrating the metal surface. The trend of the R_t values for the functional organosilane coatings is in total agreement with the potentiodynamic studies. A lower value of C_c (higher capacitive impedance) indicates a dense film possessing low permittivity and, hence, improved corrosion resistance. The protective effects of these coating films decreased in the following order: 1M (0.15μF·cm^2) > 1G (0.26μF·cm^2) >

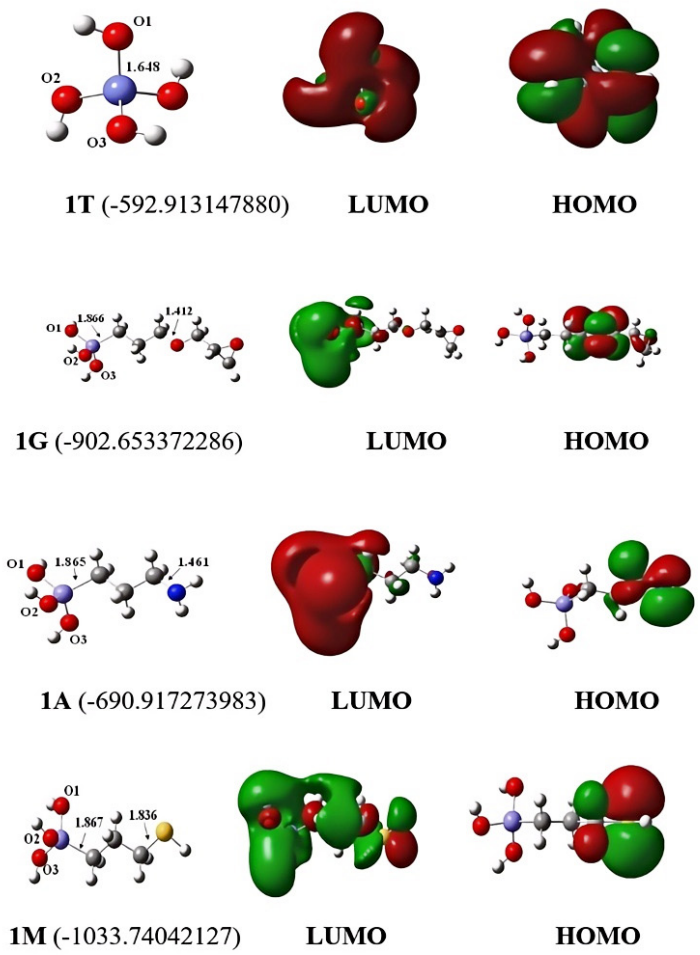

Figure 7. For Molecules 1T, 1G, 1A, and 1M, Optimized Geometries and Significant Kohn–Sham Molecular Orbitals (in the Gas Phase) Are Shown. The atoms represented by the colours red, violet, grey, white, blue, and yellow are O, Si, C, H, N, and S, respectively. The total energy (in Hartree) of each molecule is presented in parentheses.

Table 4. Mulliken[$] Charges (In e$^-$) of the Atoms/Groups in the 1t-1g Silane Molecule

Molecules	Si	O1	O2	O3	End atoms
1T	+1.3	-0.6	-0.6	-0.6	-0.8 (O)
1G	+1.3	-0.8	-0.8	-0.8	-0.3 (O)
1A	+1.3	-0.8	-0.8	-0.8	-0.8 (N)
1M	+1.3	-0.8	-0.8	-0.8	-0.1 (S)

Notes: [$]DFT (B3PW91)/6-311G* calculations

1A (1.11μF·cm^2) > 1T (9.83μF·cm^2). This indicates that the thiol-functionalized organosilane provides good interfacial adhesion compared to epoxy and amine-functionalized silanes. This can be explained by the logic that atoms with higher electron negative values tend to form strong chemical bonds with hydrogen atoms. However, oxygen-bearing epoxy functional groups are supposed to provide strong bonding compared to thiol-bearing functional groups. Moreover, quantum chemical studies (explained in the next section) have further shown that thiols are the best adhesion promotors in terms of the electronic structures of organosilane compounds and global reactivity parameters.

3.4 Quantum Chemical Studies

Figure 7 displays the optimized molecular structures with total energies and the distributions of the lowest unoccupied molecular orbital (LUMO) and highest occupied molecular orbital (HOMO) of the compounds under investigation in the gas phase. Table 4 summarizes the Mulliken charges of the atoms in each of the four organosilane compounds, and Table 5 summarizes the quantum chemical characteristics.

The capacity of a molecule to donate electrons to an empty molecular orbital of another metal is represented by the energy of HOMO (E_{HOMO}) according to frontier molecular orbital (FMO) theory. On the other hand, the electron affinity of E_{LUMO} (the energy of the LUMO) is related to a molecule's tendency to take up electrons. The adsorption centers of coating molecules can also

Table 5. Quantum Chemical Parameters[$] (in Gas/water) for Organosilanes Molecules

Molecules	E_{LUMO} (eV)	E_{HOMO} (eV)	ΔE (eV)	η (eV)	χ (eV)	ΔN (€)	μ (D)
1T	1.2/1.1	-7.7/-7.9	8.9/9.0	4.4/4.5	3.2/3.4	0.08/0.00	0.02/0.02
1G	0.5/0.8	-7.2/-7.3	7.7/8.0	3.8/4.0	3.3/3.2	0.16/0.07	3.2/3.8
1A	0.6/0.8	-6.4/-6.6	7.0/7.4	3.5/3.7	2.9/2.9	0.21/0.10	2.3/3.0
1M	0.4/0.4	-6.4/-6.7	6.9/7.1	3.4/3.6	3.0/3.2	0.20/0.08	3.4/4.2

Notes: [$]DFT (B3PW91)/6-311G* calculations

be predicted using FMO. The HOMO and LUMO of the four different silane molecules in Figure 6 have separate distribution centers, implying that the functional group attached to the alkyl chain influences the four molecules' collective reactivity. Infrared spectroscopy has proven that the functional groups of organosilane molecules can give electrons to create chemical bonds with the metal of the substrate. HOMOs in 1G, 1A, and 1M molecules are typically found on terminal functional groups like epoxy, amine, and thiol. This indicates that adsorption on the metal surface happens via end functional groups[60]. For 1T, the HOMO is distributed in the Si-O bonds. As illustrated in Figure 7, the LUMO distributions of 1G, 1A, and IT are comparable and primarily dispersed in the Si-O bond. Because the Si-O bond and thiol group have the same charge density as the LUMO in 1M, thiol is a good electron acceptor for producing a back-donation interaction with metal, allowing 1M molecules to adsorb on the metal surface. Table 4 presents the Mulliken atomic charges of the main atoms in the four organosilane compounds.

There are no differences in the negative charges of O atoms directly connected to the Si center in 1G, 1A, and 1M, indicating that the reactivity of alkyl chains connected to the Si center is similar in 1G-1M, although different functional groups are attached at the end. Differences in charges come at the end atoms associated with the alkyl chain for different functional groups in 1G-1M. These negatively charged terminal atoms will aid in the adsorption process in molecules 1G, 1A, and 1M. The atomic charges of the two O-terminal atoms in 1G are -0.3, those of N are -0.8 in 1A, and those of S are -0.1 in 1M.

3.4.1 Global Reactivity Parameters

In general, a high value of E_{HOMO} and a low value of E_{LUMO} indicate that this molecule effectively inhibits metal corrosion[61]. The interaction between the adsorbed molecule and the substrate surface is quantified by the chemical stability of the metal complex, which is determined by the gap between the HOMO and LUMO energy levels of the molecule ($\Delta E=E_{LUMO}-E_{HOMO}$). Taking an electron out of the last available orbital, the excitation energy must be small; hence, molecules with low ΔE values have better inhibitory efficacy. A highly reactive and kinetically unstable molecule is typically characterized by a low ΔE and increased polarizability. This type of molecule is known as a "soft molecule"[62,63]. In table 5, the values of E_{HOMO} in both the gas and aqueous phases follow the order of 1M≈1A>1G>1T, while the values of E_{LUMO} follow the order of 1M<1G<1A<<1T. The trend of the ΔE values in Table 5 is 1M<1A<1G<<1T for both the gas and solution phases. Based on the above results and explanations, the effectiveness of inhibiting corrosion (in gaseous and aqueous phases) by four organosilane molecules follows the order of 1M>1A>1G>1T. It can be observed that the four compounds' respective corrosion inhibition efficiencies 1G-1T decrease in the aqueous phase compared to those in the gas phase due to the higher E_{LUMO}, lower E_{HOMO}, and higher ΔE values in the aqueous phase than in the gas phase.

The stability and reactivity of a molecule can be predicted using the global hardness η (equation (2)). The ΔE value of a hard molecule is high, while that of a soft molecule is low. Soft molecules are more reactive than their rigid counterparts because they can more easily donate electrons to an acceptor. The molecules of the coating are Lewis bases, while the metal is a Lewis acid in this case. According to the HSAB (hard soft acid base) theory[64], since most metals are weak acids, the most efficient way to prevent corrosion is to use soft base molecules. Therefore, the most efficient corrosion prevention method involves molecules with the lowest global hardness[65]. Table 5 clarifies that the η values in the gas and aqueous phases are in the following order: 1M≈1A<1G<1T. According to all of these findings, the investigated organosilane molecules' order of corrosion inhibition efficacy is 1M≈1A>1G>1T, meaning that the best organosilanes for protecting metals from corrosion are those that include amino and mercapto functional groups. Because all molecules have larger η values in the aqueous phase than in the gas phase, it should be noted that the inhibitory efficiency of molecules is lower in the aqueous phase than in the gas phase.

The study is shown in Table 5, where the number of electrons transferred (ΔN) between four organosilane molecules and a metal substrate was calculated using equation (5). Sanderson's electronegativity/hardness equalization principle[66], provides the basis for the descriptor ΔN, which signifies that electron interaction between the coating and metal molecules will persist until their electronegativity levels are equal. When ΔN is positive, the coating molecule functions as an electron donor, and as ΔN increases, the corrosion rate

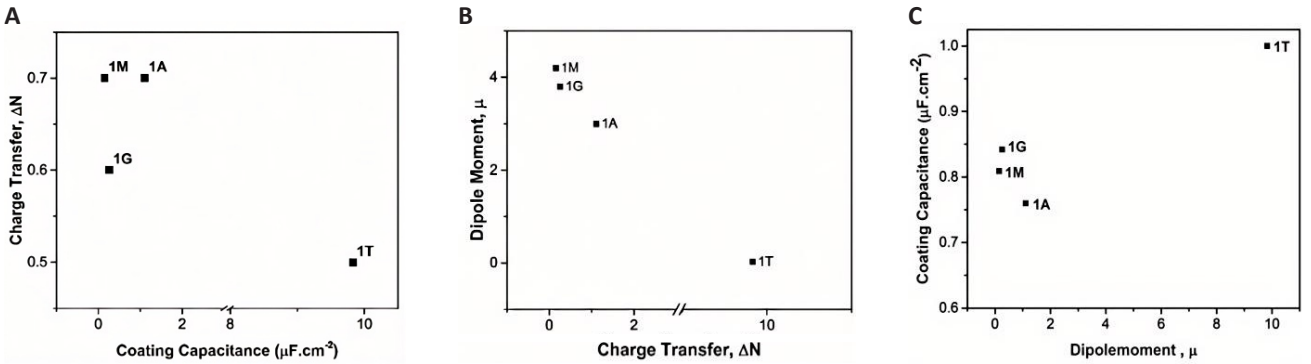

Figure 8. The Trends of the Curve Using Capacitive Impedance from the Experiments and the ΔN and μ Values from the Quantum Chemical Calculations Mutually. Variation of (A) charge transfer with coating capacitance, (B) dipole moment with charge transfer, and (C) coating capacitance with the dipole moment.

falls because the metal and molecule have a stronger interaction. The strongest metal-silane linkages may be produced by organosilanes with thiol and amino functional groups, as shown in Table 5.

The dipole moment of a coating molecule is another measure of its efficacy as a corrosion barrier. It plays a crucial role in determining a molecule's polarity. Increasing the dipole moment improves the efficiency of corrosion[67,68] because it makes it easier for the molecule to adsorb on the inorganic substrate surface via physical forces. The values of molecules 1G, 1 M, and 1A are all greater than that of water (1.88D), as shown in Table 5. Therefore, all these molecules with functional groups are expected to be strongly adsorbed on the substrate surface through physical forces, which agrees with the FTIR results described in the experimental section. The order of the μ values is 1M>1G>1A regardless of the phase, indicating that the 1M organosilane molecule containing a thiol functional group provides the strongest adsorption through physical forces onto the GI steel substrate compared to that for other silanes.

Overall, based on the quantum chemical calculations of the global descriptors considered for each molecule as described above, the order of the efficiencies of the coating molecules against the corrosion of GI steel is 1M≈1A>1G>>1T. These results establish that functional organosilanes such as MPTMS, APTES, and GPTMS offer much better corrosion protection to GI steel than do normal silanes such as TEOS. All these computational results are in good agreement with the experimental results. The trends of the curve using capacitive impedance from the experiments and the ΔN and μ values from the quantum chemical calculations mutually satisfy the observation, as shown in Figure 8.

Figure 8A and 8B show the variation of charge transfer with coating capacitance and dipole moment, respectively, whereas Figure 8C shows the variation of coating capacitance with the dipole moment of the different silane-coated systems. The stronger the dipole moment of the molecules in the material, the greater the capacitance. There is marginal change in coating capacitance in case of 1A, 1M and 1G. However, coating capacitance of 1T is higher due to its larger dipole moment. A higher charge transfer and dipole moment indicate better protection of GI steel against corrosion, which is also evident from the lower coating capacitance shown in Figure 8A. The coating capacitance for the functional silane coatings (1G, 1 M, 1A) is almost 10 orders of magnitude lower than that of the nonfunctional silane coating (1T). The 1M coating offers the highest impedance, which reflects the higher corrosion resistance observed in the potentiodynamic studies as well.

3.4.2 Adsorption of Organosilanes on the $(ZnO)_{12}$ Cluster

The $(ZnO)_{12}$ nano-cluster, which served as a model for the top surface of GI steel that really interacts with coatings, was used to study the adsorption process at the interface between organosilanes and ZnO nano-cluster. Figure 8 presents the optimized ground state geometry of the $(ZnO)_{12}$ cluster together with key Kohn-Sham orbitals of the cluster. The cage-type optimized $(ZnO)_{12}$ cluster has two different types of Zn-O bonds: one larger (bond distance: 1.98 Å) and the other shorter (bond distance: 1.92 Å)[21,69]. O (2p) and Zn (3d) orbitals constituted the majority of the HOMO, whereas the antibonding overlap between O (2S) and Zn (4S) orbitals was present in the LUMO. The calculated difference between the cluster's HOMO and LUMO orbitals was 4.15 eV. The optimized form of the ZnO_{12} nano-cluster exhibited good agreement with previous DFT analyses[56]. The optimized structures of adsorbed organosilanes 1T@$(ZnO)_{12}$, 1G@$(ZnO)_{12}$, 1A@$(ZnO)_{12}$, and 1 M@$(ZnO)_{12}$ at the ground state level are presented in Figure 9. Each adsorbed geometry was fully relaxed during DFT geometry optimization, where organosilane molecules were placed on the ZnO cluster by targeting heteroatoms. The electron densities in Mos and atomic charges of organosilane molecules clearly proved that the heteroatoms are the probable adsorption centers, as explained above.

Equation (11) was utilized to compute the adsorption energies (E_{ads}), where E_{ZnO} represents the overall energy

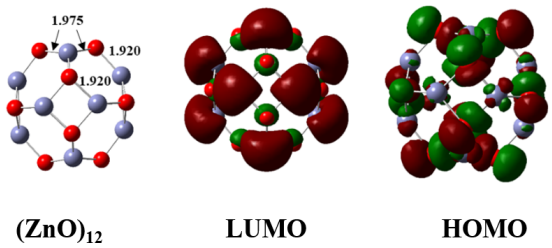

Figure 9. Optimized Geometries and Important Kohn–Sham Molecular Orbitals of the $(ZnO)_{12}$ Cluster. The colors red and violet refer to O and Zn atoms, respectively. The bond distances are in Å.

Table 6. E_{LUMO} And E_{HOMO}, Gap Between Homo and Lumo Orbitals ($\triangle E$), and Adsorption Energy (E_{ads}) in Gas Phase

Molecules	E_{LUMO} (eV)	E_{HOMO} (eV)	$\triangle E$ (eV)	E_{ads} (kcal/mol)
$(ZnO)_{12}$	-3.15	-7.31	4.15	-
$1T@(ZnO)_{12}$	-3.04	-7.15	4.11	-5.1
$1G@(ZnO)_{12}$	-2.70	-6.76	4.05	-41.0
$1A@(ZnO)_{12}$	-2.66	-6.65	3.99	-43.6
$1\ M@(ZnO)_{12}$	-2.67	-6.87	4.20	-47.9

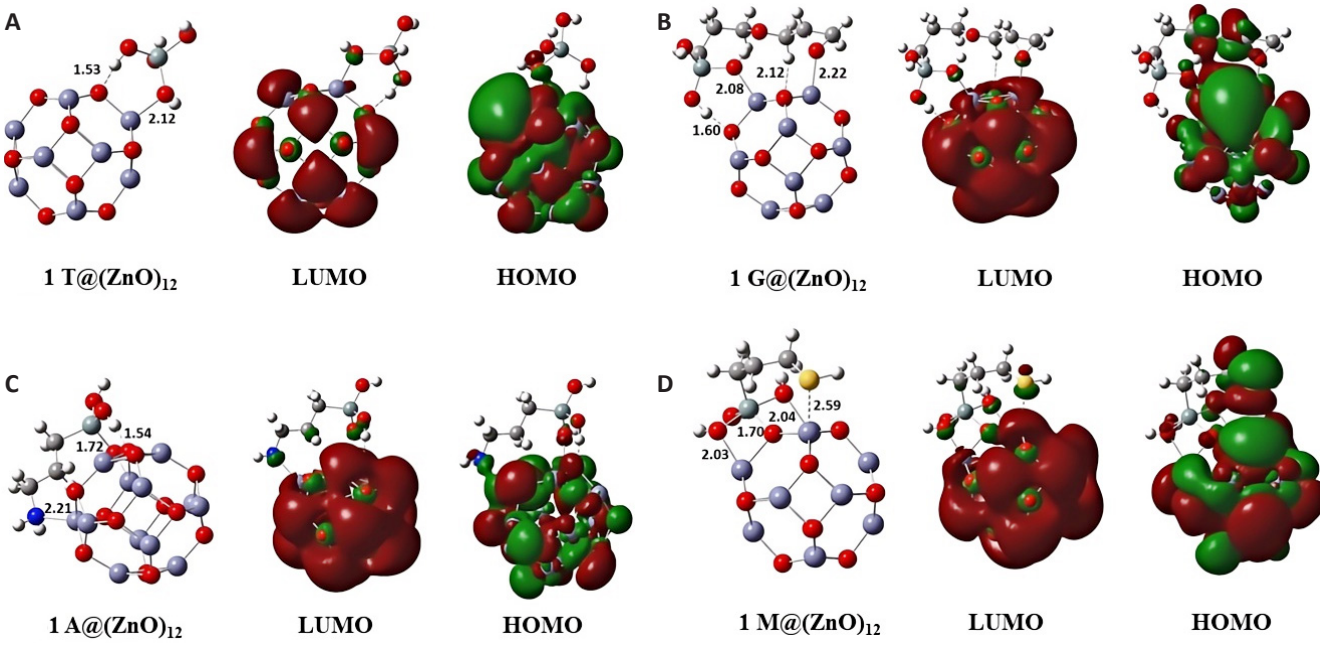

Figure 10. Adsorption Configuration onto the $(ZnO)_{12}$. A: Cluster of TEOS; B: Cluster of GPTMS; C: Cluster of APTES, and D: Cluster of MPTMS. Colours red, violet, cyan, grey, white, blue, and yellow refer to O, Zn, Si, C, H, N, and S atoms, respectively.

of the optimized $(ZnO)_{12}$ cluster, E_{Si} denotes the overall energy of the optimal organosilane molecule, and $E_{ZnO\text{-}Si}$ represents the overall energy of the optimized adsorbed structures. Table 6 provides the adsorption energies (E_{ads}) of each adsorbed structure as well as the energies of critical molecular orbitals and gaps between HOMO and LUMO orbitals.

$$E_{ads} = E_{ZnO-Si} - (E_{ZnO} + E_{Si}) \qquad (11)$$

Every organosilane molecule experienced an exothermic adsorption process. The adsorption energy range (E_{ads}) was found to be between 5.1 and 47.9kcal/mol. The E_{ads} order was $1T@(ZnO)_{12} << 1A@(ZnO)_{12} < 1G@(ZnO)_{12} < 1M@(ZnO)_{12}$, indicating a substantially higher exothermic adsorption process for functional organosilane molecules than for non-functional organosilane molecules. The strong adsorption of three functional organosilanes onto the $(ZnO)_{12}$ nano-cluster was verified by high values (>40kcal/mol) of E_{ads}.

Functional organosilane molecules adsorbed via multiple bond formations with the ZnO cluster. Bonding interactions formed between Zn atoms of cluster and heteroatoms O, N, and S present in the organosilanes, as shown in (Figure 10B-D), where the $Zn\text{-}_O$ bond distance was approximately 2.1Å. The Zn-N distance was 2.2Å in the adsorption of 1A (Figure 10B), and the Zn-S distance was 2.6 Å in the adsorption of 1M (Figure10C). The silicon center underwent five coordinations and became hypervalent through Si-O bond formations with the O atom of the ZnO cluster in adsorption of 1A and 1 M. The Si-O bond distance was 1.7Å in adsorptions of 1A and 1M. O---H-C hydrogen bonding interactions were observed during the adsorption of 1G between the H atom connected to the C atom adjacent to the epoxy group and the O atom of the cluster. The H atoms of the OH groups formed hydrogen bonds with the O atom of the ZnO cluster, where O---H bond distance is 1.5Å in adsorption of 1T, 1G, and 1A. The hypervalency of heavier Group 14 elements has been reported in previous theoretical studies[27]. All these bonding interactions supported the formation of $Si\text{-}O_{surface}$, $Zn\text{-}O_{molecule}$, O-H, Zn-N, and Zn-S bonds during

Table 7. Natural Charges (in e) of Important Groups and heteroatoms in Alkyl Chain of Organosilanes for the Adsorbed Structures

Molecule	$(ZnO)_{12}$	Organosilane	Si	O1	O2	O3	Heteroatoms
1T@$(ZnO)_{12}$	-0.04	+0.04	+2.22	-1.06	-1.06	-1.03	-1.03 (O)
1G@$(ZnO)_{12}$	-0.14	+0.14	+2.19	-1.12	-1.06	-1.10	-0.60 (O)
1A@$(ZnO)_{12}$	-0.16	+0.16	+2.19	-1.11	-1.09	-1.06	-0.87 (N)
1 M@$(ZnO)_{12}$	-0.12	+0.12	+2.15	-1.10	-1.08	-1.05	+0.03 (S)

the adsorption of organosilane molecules onto the $(ZnO)_{12}$ cluster.

As shown in Table 7, natural charges of adsorbed geometries showed that the organosilane moiety is positively charged and that the $(ZnO)_{12}$ cluster is negatively charged. This result claimed that electron donation occurred from the organosilane moiety to the $(ZnO)_{12}$ cluster during adsorption.

When comparing the adsorption of functional organosilanes to that of non-functional ones, the positive charge of the organosilane moiety increased. This suggests that the presence of O/N/S heteroatoms in the alkyl chain facilitates the donation of electrons from the organogermane moiety to the $(ZnO)_{12}$ cluster during the adsorption process. The greater ΔN values of 1G, 1A, and 1M compared to 1T were justified by this outcome. The S atom's positive charge significantly increased during the 1M adsorption (Table 6), suggesting that the S atom actively contributed to the electron donation from the organosilane during adsorption. Key Kohn-Sham molecular orbitals for the adsorbed structures are presented in Figure 3B, C and Figure 4A, B. These MOs further shed light on electron donation by organosilane moieties. LUMOs were located mainly on the $(ZnO)_{12}$ cluster, while the HOMOs consisted of overlap of electron densities between the cluster and organosilane moieties. All these results showed that chemical bonds formed at the interface for functional silanes, which is supported by larger values of the E_{ads} of functional silanes.

The higher adsorption energies of the functional organosilanes (1G, 1A, and 1M) than of the nonfunctional organosilane (1T) are attributed to their higher E_{HOMO} energies and lower ΔE values than those of the nonfunctional organosilane, which favors electron donation from the HOMOs of the organosilane to the LUMOs of the ZnO substrate.

4 CONCLUSIONS

This study aimed to assess the corrosion protection efficiency of functionalized (-O-, $-NH_2$, -SH) and nonfunctionalized organosilane films applied to GI steel. The best protection (92.5%) was given by the thiol-functionalized organosilane coating (1M), which outperformed the epoxy (1G), amino-functionalized (1A), and nonfunctionalized (1T) coatings. Capacitive and resistive impedances were greater in the 1M film, suggesting better corrosion inhibition and barrier qualities against corrosive ions. The study examined the relationship between the electronic structure of the organosilane molecules and corrosion inhibition efficacy using DFT method. Functional groups such as epoxy, amine, and thiol are thought to be the means of adsorption to the $(ZnO)_{12}$ cluster, according to frontier orbitals and Mulliken atomic charges in 1G, 1M, and 1A. The ΔN values followed the trend 1A≈1M>1G≈1T in both gas and aqueous phases, indicating strong metal-silane coordinate bond formation in 1A and 1M. The order of μ values was 1M>1G>1A>>1T, suggesting that functional organosilanes adsorb more strongly to the GI steel than nonfunctional silanes through physical forces. This DFT research on the interactions between organosilane molecules and a $(ZnO)_{12}$ cluster found numerous bond forms at the interface during adsorption. The heteroatoms (O/N/S) in organosilane molecules strongly bind with Zn atoms, facilitating the adsorption process. The silicon core in molecules 1A and 1M becomes hypervalent, coordinating with five atoms. Adsorption is exothermic for all compounds, showing great potential for adsorption onto the ZnO substrate. The adsorption energies (E_{ads}) surpass 40kcal/mol, with the order of adsorption energy being 1T@$(ZnO)_{12}$<<1G@$(ZnO)_{12}$<1A@$(ZnO)_{12}$<1M@$(ZnO)_{12}$. Functional organosilanes have substantially greater adsorption energies than nonfunctional ones, ascribed to higher E_{HOMO} energies and lower ΔE values, enabling electron donation from the organosilane HOMOs to the ZnO LUMOs. Evidence of chemical bond formation at the interface is supported by electron density overlap in the molecular orbitals, and natural charge analyses indicate significant charge transfer from the organosilane moiety to the $(ZnO)_{12}$ cluster.

Acknowledgements

We are deeply grateful to Tata Steel Ltd., Jamshedpur, India, for providing the funding and granting us permission to publish this work. We express our gratitude to all of our technical personnel and especially to Mrs. Priyanka Pandey for her assistance with the SEM.

Data Availability

Since these data are also part of an ongoing investigation, their raw/processed versions cannot be provided at this time.

Conflicts of Interest

The authors declared no conflict of interest.

Author Contribution

Badaik S was responsible for the original draft preparation, conducting experimental work, data curation, and data analysis. Ray M contributed to review and editing the draft, as well as DFT modeling. Ghosh R took on roles in conceptualization and investigation. Nidhi M assisted in review, editing, and data analysis. Nayak S provided support in reviewing and editing the manuscript. Bhagat AN also contributed through writing review and editing. Ambade B participated in the review and editing process. Reddy SRM was involved in the review and editing of the manuscript. Lastly, Rout TK led the project's conceptualization and supervision and participated in review and editing of the writing.

Abbreviation List

APTES, 3-aminopropyltriethoxysilane
DFT, Density functional theory
ECP, Effective core potential
EIS, Electrochemical impedance spectroscopy
FMO, Frontier molecular orbital
FTIR, Fourier transform infrared
GI, Galvanized
GPTMS, 3-glycidoxypropyltrimethoxysilane
HOMO, Highest occupied molecular orbital
LUMO, Lowest unoccupied molecular orbital
MPTMS, 3-mercaptopropyltrimethoxysilane
NBO, Natural bond order
SCRF, Self consistent reaction field
TEOS, Tetraethoxysilane
VOC, Volatile organic compound

References

[1] Dennis RV., Patil V, Andrews JL et al. Hybrid nanostructured coatings for corrosion protection of base metals: A sustainability perspective. *Mater Res Express*, 2015; 2: 032001.[DOI]

[2] Talebian N, Kheiri M. Sol-gel derived nanostructured nickel oxide films: Effect of solvent on crystallographic orientations. *Solid State Sci*, 2014; 27: 79-83.[DOI]

[3] Gharbi O, Thomas S, Smith C et al. Chromate replacement: what does the future hold?. *NPJ Mat Degrad*, 2018, 2: 12.[DOI]

[4] Zaferani SH, Peikari M, Zaarei D et al. Using silane films to produce an alternative for chromate conversion coatings. *Corrosion*, 2013; 69: 372-387.[DOI]

[5] Tanglumlert W, Prasassarakich P, Supaphol P et al. Hard-coating materials for poly (methyl methacrylate) from glycidoxypropyltrimethoxysilane-modified silatrane via a sol - gel process. *Surf Coat Tech*. 2006; 200: 2784-2790.[DOI]

[6] Talha M, Wang Q, Xu M et al. Improved corrosion protective performance of hybrid silane coatings reinforced with nano ZnO on 316 L stainless steel. *Colloid Interfac Sci*, 2021, 42: 100411.[DOI]

[7] Steel C. Preparation of Sol-Gel Derived Anticorrosive Coating 2019.

[8] Subramanian V, Ooij WJV. Effect of the Amine Functional Group on Corrosion Rate of Iron Coated with Films of Organofunctional Silanes. *Corrosion*, 1998: 204-215.[DOI]

[9] Matinlinna JP, Lassila LV. Enhanced resin-composite bonding to zirconia framework after pretreatment with selected silane monomers. *Dent Mater*, 2011; 27: 273-280.[DOI]

[10] Aziz T, Ullah A, Fan H et al. Recent Progress in Silane Coupling Agent with Its Emerging Applications. *J Polym Environ,* 2021; 29 : 3427–3443.[DOI]

[11] Toukal L, Keraghel S, Benghanem F et al. Electrochemical, Thermodynamic and Quantum Chemical Studies of Synthesized Benzimidazole Derivative as an Eco- Friendly Corrosion Inhibitor for XC52 Steel in Hydrochloric Acid. *Int J Electrochem Sci*, 2018; 13: 951-974.[DOI]

[12] Olasunkanmi LO, Kabanda MM, Ebenso EE. Quinoxaline derivatives as corrosion inhibitors for mild steel in hydrochloric acid medium: Electrochemical and quantum chemical studies. *Phys E*, 2016;76:109-126.[DOI]

[13] Kumar S, Vashisht H, Olasunkanmi LO et al. Experimental and theoretical studies on inhibition of mild steel corrosion by some synthesized polyurethane tri-block co-polymers. *Nat Publ Gr*, 2016; 6: 1-18.[DOI]

[14] Fan H, Ding M, Cheng Y et al. Progress in Organic Coatings Quantum chemical studies on the inhibitive e ff ect of silane derivatives. *Prog Org Coat*, 2019; 126: 92-96.[DOI]

[15] Obot IB, Macdonald DD, Gasem ZM. Density functional theory (DFT) as a powerful tool for designing new organic corrosion inhibitors: Part 1: An overview. *Corros Sci*, 2015; 99:1-30.[DOI]

[16] Kumar H, Yadav V, Saha SK et al. Adsorption and inhibition mechanism of efficient and environment friendly corrosion inhibitor for mild steel : Experimental and theoretical study. *J Mol Liq,* 2021; 338: 116634.[DOI]

[17] Miyazaki M, Kanegae Y, Iwasaki T. Adhesion analysis of silane coupling agent/copper interface with density functional theory. *Mech Eng J*, 2014; 1: 1-10.[DOI]

[18] Kaleva A, Saarimaa V, Heinonen S et al. Dissolution-Induced Nanowire Synthesis on Hot-Dip Galvanized Surface in Supercritical Carbon Dioxide. *Nanomaterials*, 2017; 7:1-8.[DOI].

[19] Shmait A, Awad R, Rahal HT et al. Studies on coatings containing nano-zinc oxide for steel protection. *Mater Corros*, 2021, 72: 859-867.[DOI]

[20] Kathavate VS, Pawar DN, Bagal NS et al. Role of nano ZnO particles in the electrodeposition and growth mechanism of phosphate coatings for enhancing the anti-corrosive performance of low carbon steel in 3.5% NaCl aqueous solution. *J Alloy Compd*, 2020, 823: 153812.[DOI]

[21] Ray M, Saha B, Rout TK et al. Reactivity of organogermanes with ZnO substrate. *J Organomet Chem*, 2024; 1006: 123002.[DOI]

[22] Mukherjee R, Badaik S, Pandey AK et al. A hybrid coating of organometallic complex with a silane coupling compound to protect galvannealed (GA) steel from white rust without sacrificing weldability. *Mater Chem Phys*, 2023; 309: 128292.[DOI]

[23] Becke AD, Becke AD. A new mixing of Hartree-Fock and local densityfunctional theories. *J Chem Phys*, 1993; 1372.[DOI]

[24] Ray M, Nakao Y, Sato H et al. Silapropargyl / Silaallenyl and Silylene Acetylide Complexes of $[Cp(CO)_2W]^+$. Theoretical Study of Their Interesting Bonding Nature and Formation Reaction. *J Am Chem Soc*, 2006: 11927-11939.[DOI]

[25] Ray M, Nakao Y, Sato H et al. Theoretical study of tungsten η^3-silaallyl/η^3- vinylsilyl and vinyl silylene complexes: Interesting bonding nature and relative stability. *Organometallics*, 2007; 26: 4413-4423.[DOI]

[26] Ray M, Nakao Y, Sato H et al. How to Stabilize η^3-Silapropargyl/Alkynylsilyl Complex of $[CpL_2M]^+$(L)=CO, PMe_3 , or PF_3 and M=W or Mo): Theoretical Prediction. *Organometallics*, 2009: 65-73.[DOI]

[27] Ray M, Nakao Y, Sato H, et al. Experimental and theoretical study of a tungsten dihydride silyl complex: New insight into its bonding nature and fluxional behavior. *Organometallics*, 2010; 29: 6267-6281.[DOI]

[28] Stephens PJ, Devlin FJ. Ab Initio Calculation of Vibrational Absorption and. *J Phys Chem*, 1995; 98: 11623-11627.[DOI]

[29] Francl MM, Pietro WJ, Hehre WJ et al. Self-consistent molecular orbital methods. XXIII. A polarization-type basis set for second-row

elements. *J Chem Phys*, 1982; 77: 3654-3665.[DOI]

[30] Dabo, Ismaila, Andrea Ferretti, Nicolas Poilvert, et al. Koopmans' condition for density-functional theory. *Phys Rev B Conden Ma P*, 2010; 82 :115121.[DOI]

[31] Hehre WJ, Lathan WA. Self-Consistent Molecular Orbital Methods. XIV. An Extended Gaussian-Type Basis for Molecular Orbital Studies of Organic Molecules. Inclusion of Second Row Elements. *J Chem Phys*, 1972; 56: 5255-5257.[DOI]

[32] Dunning TH. Gaussian basis sets for use in correlated molecular calculations. I. The atoms boron through neon and hydrogen. *J Chem Phys*, 1989; 90: 1007-1023.[DOI]

[33] Miertuš S, Tomasi J. Approximate evaluations of the electrostatic free energy and internal energy changes in solution processes. *Chem Phys*,1982; 65: 239-245.[DOI]

[34] Cossi M, Barone V, Cammi R, et al. Ab initio study of solvated molecules: A new implementation of the polarizable continuum model. *Chem Phys Lett*, 1996; 255: 327-335.[DOI]

[35] Weinhold F. Natural Bond Orbital Analysis : A Critical Overview of Relationships to Alternative Bonding Perspectives. *J Comput Chem*, 2012: 2363-2379.[DOI]

[36] Parr RG, Pearson RG. Absolute Hardness: Companion Parameter to Absolute Electronegativity. *J Am Chem Soc*, 1983; 105: 7512-7516.[DOI]

[37] Pearson RG. Absolute Electronegativity and Hardness: Application to Inorganic Chemistry. *Inorg Chem*, 1988; 27: 734-740.[DOI]

[38] Pearson RG. Chemical hardness and bond dissociation energies. *J Am Chem Soc*, 1988;110:7684–7690.[DOI]

[39] Guin AK, Nayak SK, Rout TK et al. Corrosion behavior of nanohybrid titania-silica composite coating on phosphated steel sheet. *J Coat Technol Res*, 2012; 9: 97-106.[DOI]

[40] Li S, Wang J, Ye Y et al. Composite Si-O-metal network catalysts with uneven electron distribution: Enhanced activity and electron transfer for catalytic ozonation of carbamazepine. *Appl Catal B-Environ*, 2020; 263: 118311.[DOI]

[41] Longhi M, Kunstal SR, Beltrami LVR et al. Effect of Tetraethoxy-silane (TEOS) Amounts on the Corrosion Prevention. *Mater Res*, 2015; 18: 1140-1155.[DOI]

[42] Ma S. Mechanical and thermal properties and morphology of epoxy resins modified by a silicon compound. *J Macromol Sci A*, 2010, 47: 1084-1090.[DOI]

[43] Balgude D, Konge K, Sabnis A. Synthesis and characterization of sol-gel derived CNSL based hybrid anti-corrosive coatings. *J Sol-Gel Sci Technol*, 2014; 69: 155-165.[DOI]

[44] Li Y, Wang Y, Tran T et al. Vibrational spectroscopic studies of (3-mercaptopropyl) trimethoxylsilane sol - gel and its coating. *Spectrochim Acta A*, 2005; 61: 3032-3037.[DOI]

[45] Balaji J, Roh SH, Edison TNJI et al. Sol-gel based hybrid silane coatings for enhanced corrosion protection of copper in aqueous sodium chloride. *J Mol Liq*, 2020; 302: 112551.[DOI]

[46] Dagdag O, Safi Z, Erramli H et al. Adsorption and anticorrosive behavior of aromatic epoxy monomers on carbon steel corrosion in acidic solution: Computational studies and sustained experimental studies. *RSC Adv*, 2019; 9: 14782-14796.[DOI]

[47] Kahyarian A, Nesic S. Electrochimica Acta H_2S corrosion of mild steel : A quantitative analysis of the mechanism of the cathodic reaction. *Electrochim Acta*, 2019; 297: 676–684.[DOI]

[48] Oliveira JAM, de Almeida AF, Campos ARN et al. Effect of current density, temperature and bath pH on properties of Ni-W-Co alloys obtained by electrodeposition. *J Alloy Compd*, 2021, 853: 157104.[DOI]

[49] Bexell U, Grehk M, Olsson M et al. XPS and AES characterization of hydrolysed γ- mercaptopropyltrimethoxysilane deposited on Al, Zn and Al-43.4Zn-1.6Si alloy-coated steel. *Surf Interface Anal*, 2004; 36: 624-631.[DOI]

[50] Yuan W, Van Ooij WJ. Characterization of organofunctional silane films on zinc substrates. *J Colloid Interface Sci*, 1997; 185: 197-209.[DOI]

[51] Mansfeld F. Use of electrochemical impedance spectroscopy for the study of corrosion protection by polymer coatings. *J Appl Electrochem*. 1995; 25: 187-202.[DOI]

[52] Wang S, Zhang J, Gharbi O et al. Electrochemical impedance spectroscopy. Nature Reviews Methods Primers, 2021, 1: 41.[DOI]

[53] Bera S, Rout TK, Udayabhanu G et al. Comparative Study of Corrosion Protection of Sol-Gel Coatings with Different Organic Functionality on Al-2024 substrate. *Prog Org Coatings*, 2015; 88: 293–303.[DOI]

[54] Pessoa MO, Freitas BR, de Oliveira Braga J et al. Anticorrosion and adhesion performance of a monolayer and double layer silane-epoxy coating systems applied on carbon steel. *Surf Coat Tech*, 2024; 485: 130909.[DOI]

[55] Kuang J, Ba Z, Li Z et al. Applied Surface Science The study on corrosion resistance of superhydrophobic coatings on magnesium. *Appl Surf Sci*, 2020; 501: 144137.[DOI]

[56] Eider CA, Baptiste MJ, Gorka J. Effect of organic precursor in hybrid sol – gel coatings for corrosion protection and the application on hot dip galvanised steel. *J Sol-Gel Sci Technol*, 2019; 89: 264-283.[DOI]

[57] Hirschorn B, Orazem ME, Tribollet B et al. Determination of effective capacitance and film thickness from constant-phase-element parameters. *Electrochim Acta*, 2010; 55: 6218-6227.[DOI]

[58] Amand S, Musiani M, Orazem ME, et al. Constant-phase-element behavior caused by inhomogeneous water uptake in anti-corrosion coatings. *Electrochim Acta*, 2013; 87: 693-700.[DOI]

[59] Sacco A. Electrochemical impedance spectroscopy: Fundamentals and application in dye-sensitized solar cells. *Renew Sustain Energy Rev*, 2017; 79: 814-829.[DOI]

[60] Assad H, Kumar A. Understanding functional group effect on corrosion inhibition efficiency of selected organic compounds. *J Mol Liq*, 2021; 344: 117755.[DOI]

[61] Boughoues Y, Benamira M, Messaadia L, et al. Adsorption and corrosion inhibition performance of some environmental friendly organic inhibitors for mild steel in HCl solution via experimental and theoretical study. *Colloid Surface A*. 2020; 593: 124610.[DOI]

[62] Madkour LH, Elroby SK. Inhibitive properties, thermodynamic, kinetics and quantum chemical calculations of polydentate Schiff base compounds as corrosion inhibitors for iron in acidic and alkaline media. *Int J Ind Chem*, 2015; 6: 165-184.[DOI]

[63] Madkour LH, Elshamy IH. Experimental and computational studies on the inhibition performances of benzimidazole and its derivatives for the corrosion of copper in nitric acid. *Int J Ind Chem*, 2016; 7: 195-221.[DOI]

[64] Pearson RG. Acids and Bases: Hard acids prefer to associate with hard bases, and soft acids prefer to associate with soft base. *Science*, 1966, 151: 172-177. [DOI]

[65] Ebenso EE, Isabirye DA, Eddy NO. Adsorption and quantum chemical studies on the inhibition potentials of some thiosemicarbazides for the corrosion of mild steel in acidic medium. *Int J Mol Sci*, 2010; 11: 2473-2498.[DOI]

[66] Sanderson RT. Electronegativity and Bond Energy. *J Am Chem Soc*, 1983;105: 2259-2261.[DOI]

[67] Stoyanova A, Petkova G, Peyerimhoff SD. Correlation between the molecular structure and the corrosion inhibiting effect of some pyrophthalone compounds. *Chem Phys*, 2002; 279: 1-6.[DOI]

[68] Şahin M, Gece G, Karcı F et al. Experimental and theoretical study of the effect of some heterocyclic compounds on the corrosion of low carbon steel in 3.5% NaCl medium. *J Appl Electrochem*, 2008, 38: 809-815.[DOI]

[69] Chen M, Dixon DA. Machine-Learning Approach for the Development of Structure-Energy Relationships of ZnO Nanoparticles. *J Phys Chem C*, 2018; 122: 18621-18639.[DOI]